

Injector Characterization for a GOX-GCH4 Single Element Combustion Chamber

M. P. Celano, S. Silvestri, G. Schlieben, C. Kirchberger, O. J. Haidn
Institute for Flight Propulsion (LFA), Technische Universität München (TUM)

Abstract

In this paper results from experimental investigation on in a GOX/GCH4 subscale combustion chamber are presented. They provide detailed information about the thermal loads at the hot inner walls of the combustion chamber at real rocket engine conditions and pressures up to 20 bar. The present study aims to contribute to the understanding of the thermal transfer processes and to validate the in-house design tool Thermtest. Due to the complex flow phenomena linked to the use of cryogenic propellants, like extreme variation of flow properties and steep temperature gradients, in combination with intensive chemical reactions, the problem has been partially simplified by injecting gaseous oxygen (GOX) and gaseous methane (GCH4).

Nomenclature

ρ	Density [kg/m ³]	OF	Oxidizer to fuel ratio [-]
a	Inner combustion chamber width/height [m]	p	Pressure [bar]
A_{hw}	Hot wall area [m ²]	P_{cc}	Pressure combustion chamber [bar]
A_{cc}	Combustion chamber cross section [m ²]	\dot{q}_{in}	Heat flux entering the control volume [W/m ²]
A_{th}	Throat cross section [mm ²]	\dot{q}_{out}	Heat flux leaving the control volume [W/m ²]
b	External combustion chamber width [m]	\dot{q}_w	Heat flux on the chamber wall [W/m ²]
Cd	Discharge coefficient [-]	$\dot{q}_{w,corr}$	Correct heat flux on the chamber wall [W/m ²]
c	Specific heat capacity [J/kgK]	Q	Accumulated heat [W]
D_i	Inner diameter (GOX) [m]	w	GOX post wall thickness [mm]
D_o	Outer diameter (GCH4) [m]	Δt_{burn}	Burning time [s]
\dot{E}_{in}	Total energy entering the control volume [W]	T	Temperature [K]
\dot{E}_{out}	Total energy leaving the control volume [W]	T_o	Starting temperature [K]
\dot{E}_{str}	Total energy stored in the control volume [W]	v	Velocity [m/s]
h	External combustion chamber height [m]	V	Volume [m ³]
J	Momentum flux ratio [-]	VR	Velocity ratio [-]
m	Mass [kg]	x	Chamber axial coordinate [mm]

1. Introduction

Today's high performance liquid propellant rocket engines for transfer into orbit and space exploration are mostly based on well-established cryogenic propellant combinations like liquid oxygen/liquid hydrogen (LOX/LH2), due to their high specific impulse, or classical storable propellants like MMH/NTO. The demanding issues in terms of high operational and handling costs of such propellants increased the attention for hydrocarbons in pre-development of future launch vehicles [1]. LOX/hydrocarbons rocket engines have the advantage of being relatively low cost, low pollution and high performance.

Many kinds of LOX/kerosene rocket engines, such as H-1, F-1, RD-170, RD-180 were developed and manufactured successfully in the US and the former Soviet Union during 1960s. Instead LOX/methane (CH4) propellant combination has a critical gap in knowledge of detailed heat transfer characteristics and injector technology. Even if considered for rocket application at various times in the US Space program [2] and in Russia [3] - [4], LOX/methane engines are not flying yet.

One of the key parameters for the selection of hydrocarbons fuels is the cooling properties. In this context oxygen/methane is one of the most promising propellant combinations. In particular, for the use in cooling systems, the threshold value of coolant-side wall temperatures is limited by coking considerations. For methane the widely

quoted value is 970 K , higher than propane (700 K) and kerosene (590 K) [5]. Moreover, the heat transfer performance of methane is higher compared to other hydrocarbon fuels as a result of its high thermal conductivity, specific heat and low viscosity. In general, methane shows, compared to other potential candidates, better overall performance from a system point of view [6], higher specific impulse [7], no risks for human health, simple extractability from natural gases and a density six-times higher than hydrogen, when stored in liquid state at typical tank pressures.

Although several research groups have performed fundamental experimental and numerical investigations [8]–[9], only a limited amount of experimental data is available for oxygen/methane combustion at relevant combustion chamber conditions. High temperature differences between the hot combustor gases and the cooling fluid in combination with high heat transfer coefficients yield extreme heat flux levels to the combustion chamber walls. For optimal cooling design the precise knowledge of the heat transfer processes in rocket engines is mandatory. The importance of these data is confirmed by the fact that life cycle prediction of rocket engine strongly depends on the accuracy of wall temperature predictions, where an error of 40 K may lead to 50% life reduction in a cryogenic propellant rocket chamber [10]. In particular, the technology of propellant injection is central for optimal rocket combustor performance due to its effect on propellant preparation and thermal loads to the walls.

In the context of the national research program Transregio SFB/TR-40 on “Technological Foundation for the design of thermally and mechanically high loaded components of Future Space Transportation System”, two multi-injector combustion chambers have been designed for gaseous oxygen (GOX) and gaseous methane (GCH₄), respectively focusing on high pressure (up to 100 bar) and film cooling behaviour and low pressure (up to 40 bar) application of optical measurement techniques. One of the key aspects of this project is to improve the knowledge on heat transfer processes and cooling methods at representative conditions in particular on injector–injector and injector–wall interactions.

Given these justifications, the focused effort has been initiated to experimentally document the detailed wall heat flux characteristic of a gaseous oxygen/gaseous methane shear coaxial single-element injector over a range of pressures and mixture ratios.

Additionally, the wall heat flux results were used as a test case for the validation of the in-house engineering tool Thermtest [1].

2. Test specimen and experimental setup

The investigations presented were performed at the new institute’s test facility for gaseous methane and gaseous oxygen. The propellant supply systems for methane and oxygen are designed for interface pressures up to 50 bar .

In this section a description of the instrumented subscale rocket chamber, injector geometry, flow conditions and data analysis procedures, which were used for the wall heat flux characterization experiments, are presented.

A. Thrust chamber and injector element

The present test campaign was performed using a modular combustion chamber with a square cross section designed for a testing time of up to 4 s at a chamber pressure of 20 bar and mixture ratio of 3.4 . The inner chamber dimensions are shown in Table 1.

Table 1: Combustion chamber dimensions

<i>Chamber length</i>	[mm]	300
<i>Chamber width</i>	[mm]	12
<i>Chamber height</i>	[mm]	12
<i>Throat height</i>	[mm]	4.8
<i>Contraction ratio A_{cc}/A_{th}</i>	[-]	2.5

The single-element rocket combustion chamber, depicted in Figure 1, consists of two chamber segments, respectively of 174 mm and 145 mm , and a nozzle segment of 20 mm length. The nozzle differs from a usual configuration due to its rectangular cross section throat of $4.8\text{ mm} \times 12\text{ mm}$, which results in a contraction ratio of 2.5 and Mach number in the chamber of 0.24 . The thrust generated at the design point conditions is up to 200 N . The material used for the chamber segments and the nozzle segment is oxygen-free copper (Cu-HCP).

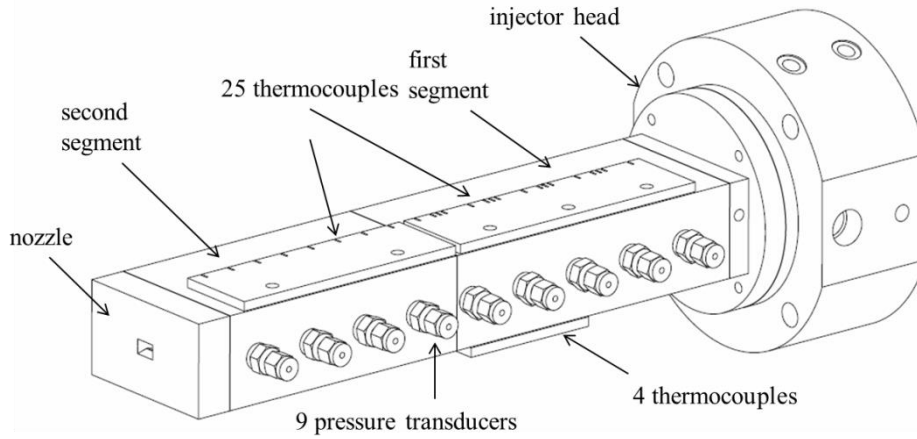


Figure 1: Combustion chamber with square cross section

To ensure uniform injection conditions, in terms of temperature and pressure, two porous plates are placed in the oxidizer and fuel manifolds respectively.

The combustion chamber is equipped with a film applicator for film cooling studies. Since this was not the focus of the present test campaign, the film applicator has been removed and substituted by a dummy. The chamber sections are held together by four tie rods having spiral springs that assure constant clamping force during thermal expansion of the chamber. The modular setup simplifies changes in chamber length or hardware configurations. Furthermore, the entire assembly is capacitive cooled in order to keep the design flexible and more accessible for temperature measurements.

The injector head of the combustor is designed to allow different injector designs. For the current study, a single shear coaxial injector element has been integrated as shown in Figure 2.

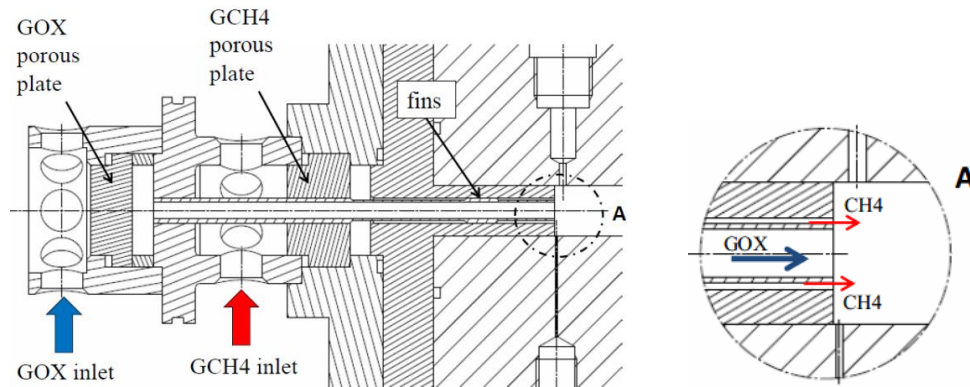


Figure 2: Single shear coaxial injector element

Previous experimental results [1] showed that configurations with the GOX post recessed have higher heat flux at the near injection-face region than GOX post flush counterparts. This indicates that the mixing cup, provided by recessing the GOX post, has a positive effect in the mixing and combustion characteristics of a shear coaxial injector. Nevertheless, for simplicity, this study omits these advancements and the GOX post is configured flush with respect to the injection face. Table 2 shows the main injector characteristic dimensions.

Table 2: Injector dimensions

<i>GOX diameter D_i</i>	[mm]	4
<i>GOX post wall thickness w</i>	[mm]	0.5
<i>GOX post recess</i>	[mm]	0
<i>GCH4 diameter D_e</i>	[mm]	6
<i>Injector area ratio A_{CH4}/A_{GOX}</i>	[-]	1.26

In order to be able to center the injector element in the faceplate, it has been equipped with four equally-spaced fins. For the current test series, the fins have been positioned with an angle of 45° to the combustion chamber center plane. The oxidizer is injected through an inner tube at velocities of about 122 m/s and the fuel, instead, through the annular gap at velocities of 132 m/s , for 20 bar , OF of 2.6 operating conditions. Shear forces between the propellants determine the mixing efficiency. Therefore, non-dimensional numbers such as the velocity ratio VR Eq. (1) and the momentum flux ratio J Eq. (2) are taken to characterize the injection conditions.

$$VR = \frac{v_{GCH_4}}{v_{GOX}} \quad (1)$$

$$J = \frac{(\rho v)_{GCH_4}}{(\rho v)_{GOX}} \quad (2)$$

Values of the velocity ratio VR and the momentum flux ratio J range from 0.89 to 1.1 and from 0.38 to 0.62 , respectively. Both the velocity ratio and the momentum flux ratio are based on propellant temperatures and pressure at injection conditions.

B. Experimental setup

The experimental setup is equipped with standard instrumentations required to characterize the operation of the chamber. For a better understanding of the complex heat transport processes, a number of equally spaced pressure transducers on the side wall provide a measurement of the static pressure distribution $p(x)$ along the chamber axis. A schematic of the combustion chamber and the associated sensor locations is given in Figure 1. WIKA A10 pressure transducers are used to record the axial evolution of the static chamber wall pressure (PC0...PC8). The pressure sensors were individually calibrated and operated at a data acquisition rate of 100 Hz .

To characterize the injection conditions, thermocouples of Type K, with 0.5 mm diameter, and pressure transducers have been installed in the chamber manifolds, prior the porous plates.

To determine the temperature field in the chamber wall three ways of thermocouple placement have been applied. The chamber segments are equipped with Type T thermocouples of 0.5 mm diameter located within the chamber wall with 1 mm , 2 mm and 3 mm distance to the hot wall. Additionally two coaxial Type T thermocouples (Medtherm) flush mounted with the hot wall and five Type K surface thermocouples attached to the external surface have been used. The Type T thermocouples and the surface thermocouples have been mounted with a regular path in the upper surface of the first and second segment, along the center plane of the combustion chamber. Instead, the Medtherm thermocouples have been press-fitted into the chamber wall, in corresponding axial positions in the lower surface of the first segment. In order to ensure better contact, the tip has been polished to match the flat surface of the chamber. The thermocouples pattern is shown in Figure 3.

The thermocouples have been inserted in precisely manufactured cylindrical holes and are kept in positions by a spring loaded system. The spring loading of the thermocouples provides a constant force of about 2 N , which ensures a continuous contact between the thermocouples tip and the base of the hole. This setup aims to minimize the chance of potential loss of contact as the material undergoes expansion and contraction due to changes in temperature or vibrations during the hot run [11]. Moreover, in order to be able to reconstruct the temperature field in the chamber material, thermocouples have been placed at different distances from the hot gas wall. Four clusters of three wall thermocouples each at a different distance d ($d1$, $d2$, $d3$) from the hot-wall are located with a constant pitch in axial direction, as depicted in Figure 4.

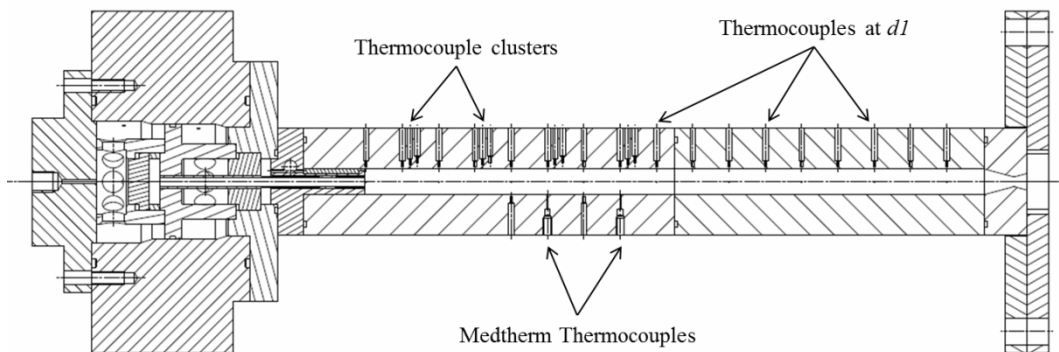


Figure 3: Thermocouple position along the combustion chamber axis

Thermocouple radial position	$d1$	$d2$	$d3$
Distance from the hot gas side [mm]	1	2	3

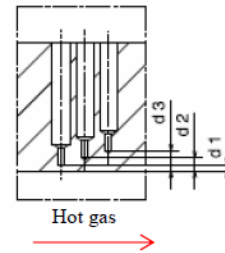


Figure 4: Thermocouple positions in the chamber wall

C. Operating conditions

The ignition of the chamber is achieved by a torch igniter using gaseous methane/gaseous oxygen, mounted to the side wall of the combustion chamber in the region near the faceplate. The mass flow rates in the combustion chamber (GCH4, GOX, GN2 for the purge) are set by sonic orifices in the feed lines and the upstream pressure. The orifices in the feed lines to the main injector were manufactured with appropriate diameters and calibrated with nitrogen using a Coriolis flow meter prior to the test campaign. For designing the operating points, the characteristic velocity c^* was calculated with CEA2 [13] and a combustion efficiency of $\eta_{c^*} = 1$ was assumed. Since the pressure values are influenced by the mass flow rates, flow checks are required in order to adjust the pressure regulators accurately. The actual mass flows have been calculated from the recorded pressure and temperature signals, gas properties and the orifice calibration data after the test. The test matrix includes testing at pressure levels from nominally 20 bar down to 5 bar and at mixture ratios of 2.6, 3.0, 3.4 and 4 (4 only for the 5 bar case). For the OF conditions, both the GCH4 and GOX mass flow rate were scaled accordantly with pressure. Figure 5 gives an overview of the planned operating points.

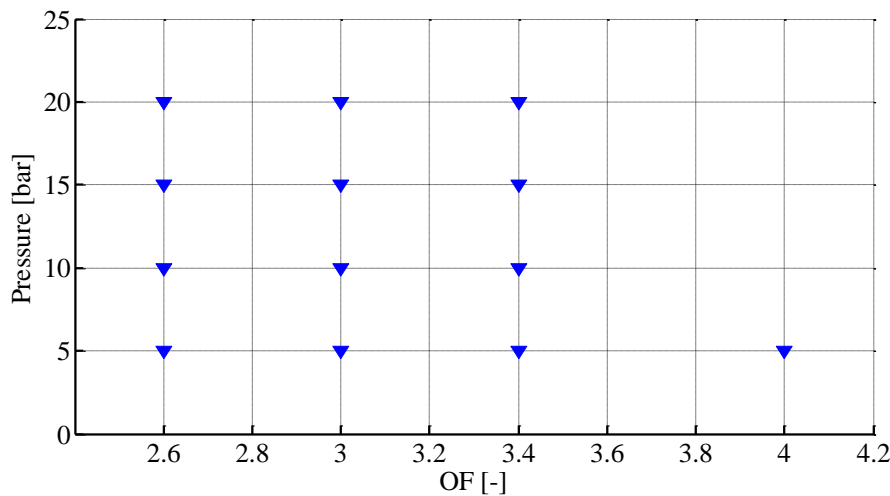


Figure 5: Test envelope – operating points

To operate the combustion chamber a test sequence was programmed into the control system. The sequence is divided into three main periods: ignition, main combustion chamber operation and shut down. Purge flows of nitrogen are activated before and after the main propellant valves are opened. To minimize the influence of the igniter on the temperature measurement, the igniter is running at minimum power for only 600 ms (200 ms prior to the opening of the main valves). The burn time of the combustion chamber was chosen to reach stable operation, required for the thermal load measurements. While the tests at 10, 15 and 20 bar were run for 3 s, the burn time for the 5 bar tests was increased to 4 s, due to the lower heat loads. Each of the operating point was run at least two times to verify the repeatability of the recorded test data. Good agreement has been obtained for all load points.

3. Experimental results and discussion

The main goal of this investigation is to determine the thermal and pressure loads distribution along the combustion chamber main axis in order to be able to characterize the injector element behavior. In the present paragraph are shown the distribution of surface temperature, the heat flux ratio and the corresponding gradients in the combustion chamber wall along the chamber axis and their transient behavior during the hot run. As an example of the test results obtained in the present test campaign, in the following section the 20 bar , $OF = 2.6$ test case is shown in more detail.

A. Temperature distribution

Surface thermocouples at different axial positions are installed for direct measurement of the local surface temperature inside the combustion chamber, whereas wall thermocouples at different distance d from the hot gas wall are used to determine the temperature field in the chamber material. The axial and radial distribution of the thermocouples allows the determination of the heat flux variation along the axis and the reconstruction of the thermal field in the chamber wall respectively.

Due to the transient nature of the problem, three time intervals have been chosen for the evaluation of the test data. A representative time interval for the starting conditions t_0 , a characteristic hot runs time step t_1 and a shutdown condition time t_2 . In the Figure 6 these time intervals are highlighted. It can also be recognized a typical temperature rise and correlated pressure build-up during hot runs.

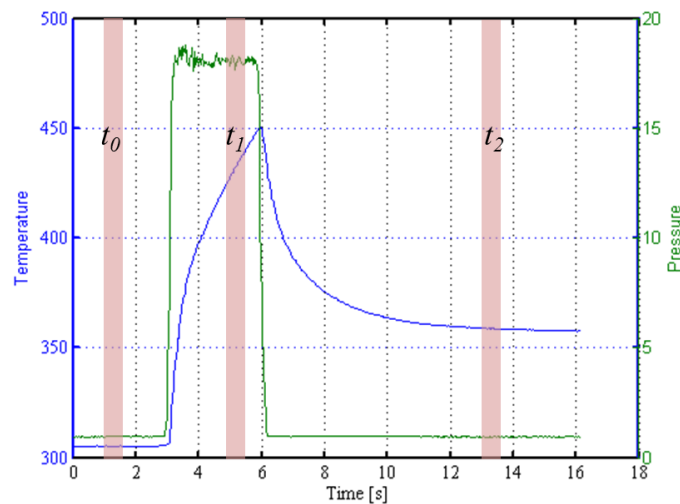
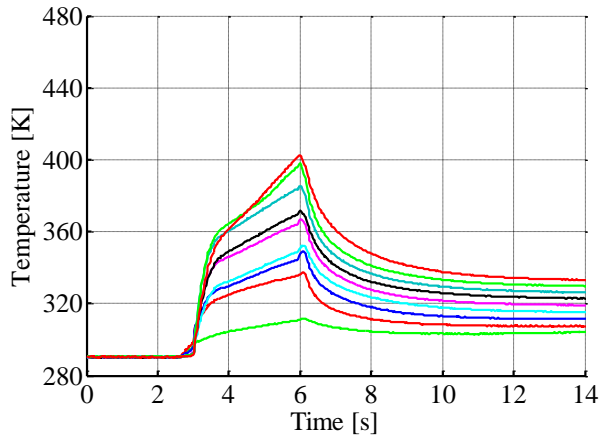
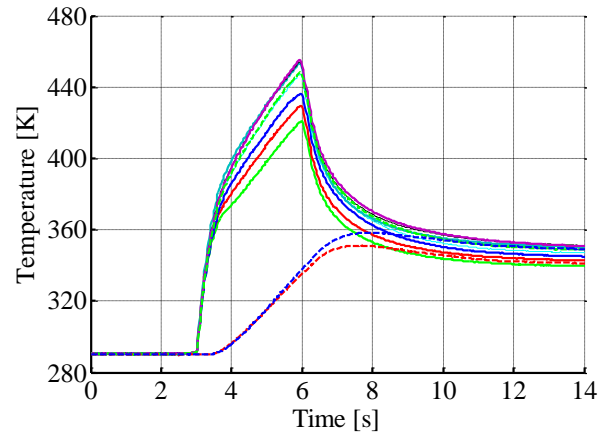
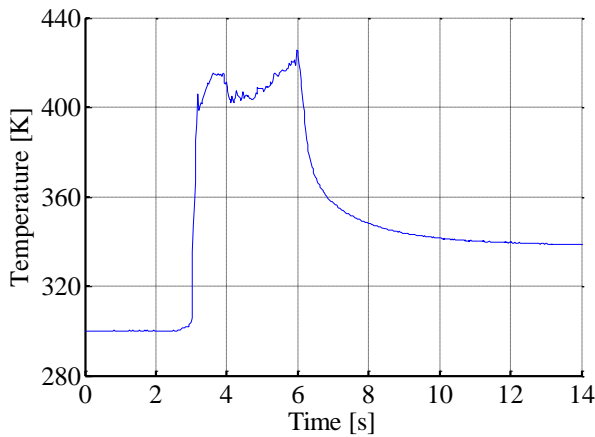
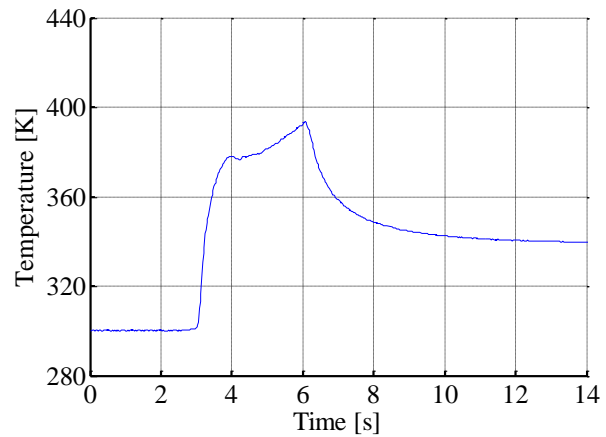


Figure 6: Temperature and chamber pressure build-up

Figure 7 and Figure 8 show the temperature reading of the 1 mm thermocouples along the chamber axis during firing. For the temperature versus time trace, two main gradients could be typically recognized: a steeper increase in the first second after ignition, as the thermal wave travels through the chamber wall, and a smoother temperature increase during the remaining running time. Furthermore it can be noticed that the slope of the wall temperature versus time profiles decreases with time into the firing. The same trend could be identified in each temperature signal in the first and second chamber segment.


 Figure 7: Thermocouple signal: 1st segment, distance $d1$

 Figure 8: Thermocouple signal, 2nd segment, distance $d1$

A non-conform behavior for higher mixture ratios (3.0 to 3.4), is exhibited from the Medtherm thermocouples positioned in the region next to the faceplate, as shown in the example in Figure 9.


 Figure 9: Medtherm temperature signal, $P_{cc} = 20 \text{ bar}$
 $OF = 3.4$, flush-mounted with the hot wall

 Figure 10: Temperature signal, $P_{cc} = 20 \text{ bar}$ $OF = 3.4$,
 2 mm from the hot wall

The temperature signal for this thermocouple increases steeper at the first 500 ms and then it decreases for a short period, before increasing with time until the end of the firing. This behavior was already observed at the Pennsylvania State University [1]. At that time it was associated to a variation of the thermal contact between the thermocouple and the chamber. Since a similar temperature trend is also observed for the thermocouples signal at distance $d1$ and even at $d2$ from the hot gas side, see Figure 10, this hypothesis was abandoned for the current test set-up. A detailed analysis showed that during the running time the temperature of the wall never overcomes the condensation temperature of the water, which can be considered as one of the main reaction products. Moreover the temperature peak has shown a sensitive response to OF changes and almost negligible variations with the combustion chamber pressure. While the mixture ratio approaches the stoichiometric value, the absolute and relative value of the peak increases, over the same time interval. Basic theoretical calculations (CEA2) for equilibrium chemical conditions show for increasing mixture ratio an increase in availability in terms of molar mass of condensable means (H_2O), while the molar mass of non-condensable products (CO, CO_2, \dots, H_2) decreases. This leads to a higher likelihood of linking the temperature peak to the formation of a condensation film that seems stable enough to generate a thermal protective layer, at least for a short interval of time. Furthermore, a visual observation of the exhaust plume at the start up indicates the presence of condensation, as seen in Figure 11 and Figure 12.

The formation of water may generate locally an increase in heat flux due to the enthalpy of vaporization and so the temperature peak. Previous studies [14] prove that the presence of a velocity field causes greater diffusion of the non-condensable gas at the interface into the bulk mixture and major diffusion of steam into the interface. This increases the steam mass fraction and the temperature at the interface in comparison with the case of lower velocities. That may explain the presence of only a short peak.

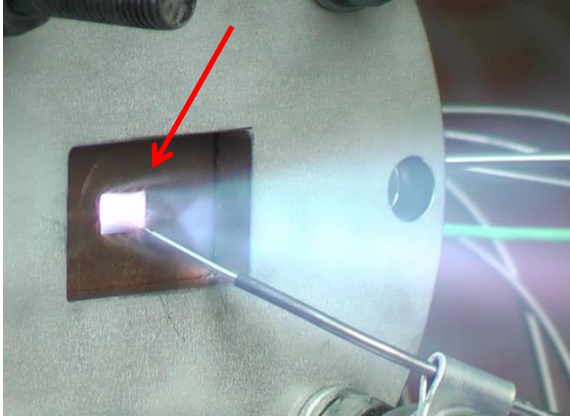


Figure 11: Exhaust plume at the start-up

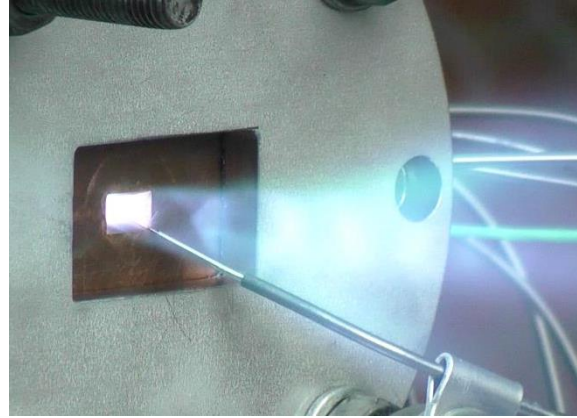


Figure 12: Exhaust plume during hot run at t_2

Due to combustion, the temperature increases steeply along the chamber axis till the accomplishment of the reaction processes. The temperature distribution along the chamber axis (dT/dx) is shown in Figure 13 for the complete set of thermocouples in the first and second segment. Since better averaging is obtained if conducted right before the end of the firing, the temperature signals have been calculated as a mean value over a 0.5 s time interval, taken at $2/3$ of the total run time (t_1). The run time is defined as the time duration, while both GCH4 and GOX propellant valves are sequenced to be opened.

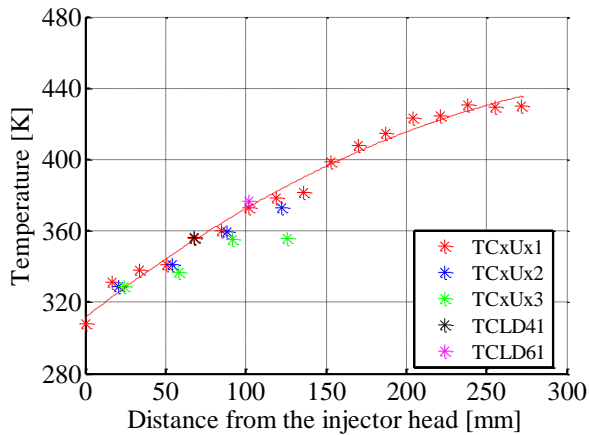


Figure 13: Temperature distribution along the chamber axis, time t_1

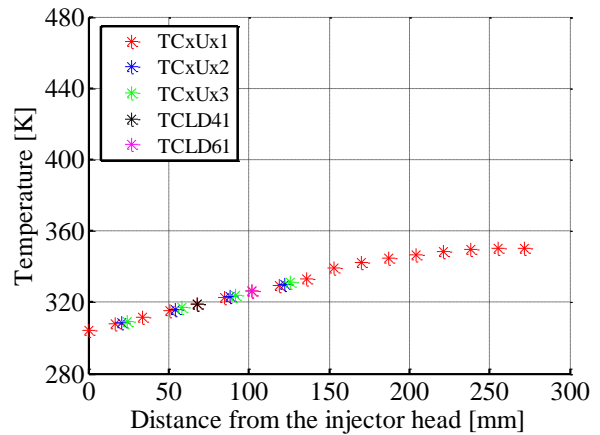


Figure 14: Temperature distribution along the chamber axis, time t_2

The curve presents a constant increase along the chamber axis till $x = 225\text{ mm}$ (where $x = 0$ is the face plate position) and a short plateau can be identified in the last section close to the nozzle, as indication of end of combustion.

Figure 14 presents the temperature readings of the thermocouples averaged over the time interval t_2 , when the thermal equilibrium is reached after shutdown. The smooth profile, typically expected at the end of combustion, prove accuracy and correct positioning of the instrumentation. Generally the temperature distribution leads to a longitudinal heat transfer from the hotter downstream section of the chamber towards the faceplate, where the temperatures are lower.

B. Heat flux

The characteristic of an injector element is mainly defined by the heat flux distribution on the hot wall along the combustion chamber axis. Due to the capacitive design of the hardware, heat fluxes can only be calculated from wall temperature measurements. Additionally, the limited test duration leads to non-stationary temperature signals. Measuring transient temperatures with sufficient accuracy for heat flux determination has been found to be challenging due to a significant sensitivity to the response time of the thermocouples.

For the present investigation a simplified 1D approach cannot be used. Due to the rectangular cross section of the combustion chamber, the temperature gradient is not significant for only one coordinate direction and it's necessary

to account for multidimensional effects. Thermal and geometrical conditions identify two relevant symmetry planes for the proposed geometry. Lines of symmetry are considered adiabatic, in the sense that there can be no heat transfer in a direction perpendicular to those lines. For the current geometry it is therefore possible to consider a simplification and analyze one-fourth of the configuration, as shown in Figure 15.

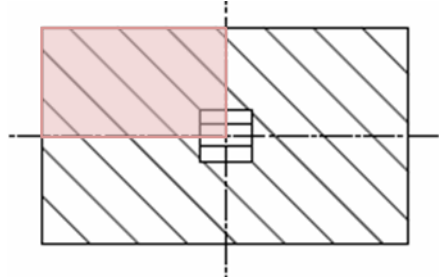


Figure 15: Control volume for heat flux calculations

At the time interval $t1$, the temperature distribution is fully established. Therefore, with the assumption of a constant heat flux, the temperature may be considered to equally change at any point of the control volume. This allows for defining the heat transfer problem only by the heat capacity of the control volume. The energy balance, including the energy storage term, is defined by:

$$\dot{E}_{in} - \dot{E}_{out} = \dot{E}_{str} \quad (3)$$

That is then possible to write in terms of heat flux as:

$$\dot{q}_{in} - \dot{q}_{out} = \frac{mc \Delta T}{A_{hw} \Delta t} \quad (4)$$

The heat flux dispersed outside the chamber, due to natural convection, can be considered negligible and the properties, density, heat capacity and conductivity of the copper, are assumed constant. The temperature variation over time ($\Delta T/\Delta t$) is calculated from the measured temperature signals during $t1$. The equation (4) can be applied at each thermocouple position, since it is independent from the temperature level. Figure 16 shows the heat flux distribution along the chamber axis at $t1$.

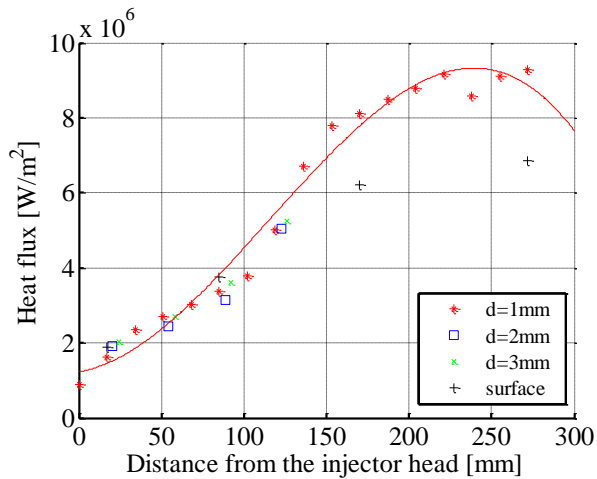


Figure 16: Heat flux distribution along the chamber axis, time $t1$

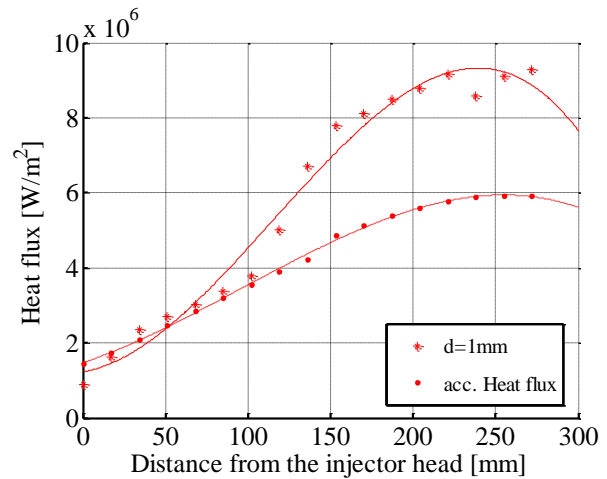


Figure 17: Heat flux distribution calculated by the accumulate heat along the chamber axis

The heat flux increases from $1 MW/m^2$, next to the faceplate up to $9 MW/m^2$, at the end of the combustion chamber. The values calculated using temperatures at different distances from the chamber wall seem to agree, and no big scattering around the trend line is featured. Also in this case, as already highlighted in the temperature trend, the signal presents a plateau in the last section upstream the nozzle, as indication of combustion end.

At the time interval $t2$, after the shut-down, the combustion chamber has reached a state, in which the temperature profile orthogonal to the chamber axis is equalized. From the longitudinal temperature profile previously presented in Figure 14 it is possible to calculate the average accumulated heat during the entire sequence. The values of the starting and final temperature can be determined at the time interval $t0$ and $t2$. The accumulated heat is defined by:

$$Q = mc[T(t2) - T(t0)] \quad (5)$$

With the equation (6) the accumulated heat can be then correlated to the heat flux during burn time at each measurement position, in order to be able to compare it with the previous method.

$$\dot{q} = C_1 \frac{[T(t_2) - T(t_0)]}{\Delta t_{burn}} \quad (6)$$

$$C_1 = \frac{bh - a^2}{4a} \rho c_v = 0.2915 * 10^6 J/(m^2 K) \quad (7)$$

Since C_1 is a constant based only on geometry and material properties, the averaged value of the heat flux can be evaluated, knowing the temperature increase. The results obtained are shown in Figure 17. It can be observed that, even if in the same order of magnitude, the values, calculated from the accumulated heat, suffer from the influence of heat losses to the environment and heat transfer in longitudinal direction to the components (i.e. manifolds and feed lines) in contact with the chamber segments.

A detailed analysis of the test data has been performed using the described procedures. Figure 18 and Figure 19 show a comparison of the heat flux along the chamber axis at time interval t_I for different chamber pressures and for different mixture ratios. In both cases the characteristic of heat release is not significantly shifted along the chamber axis. To confirm repeatability of the test results, each operating point has been performed at least two times. Test repetitions for the different load points are included in the figures and present good agreement.

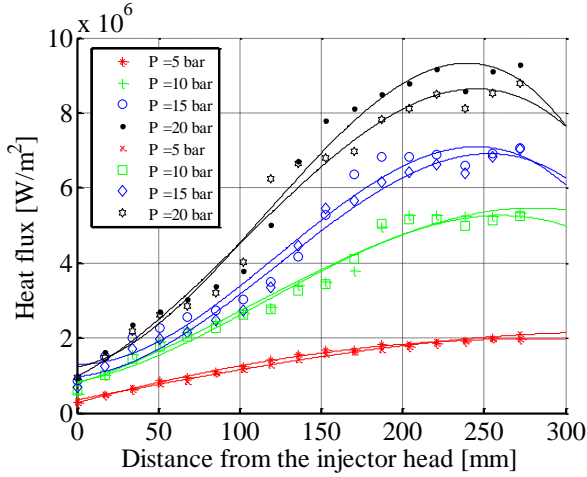


Figure 18: Heat flux distribution along the chamber axis, $OF = 2.6$ and different P_{cc} , at t_I

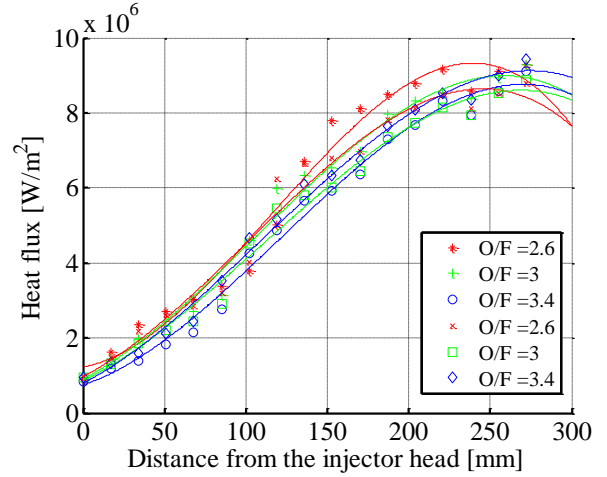


Figure 19: Heat flux distribution along the chamber axis, $P_{cc} = 20 \text{ bar}$ and different OF , at t_I

C. Pressure distribution and discharge coefficient of the injector element

The design of the presented combustion chamber allows for the implementation of a high number of pressure sensors in the side walls. The nine pressure sensors are equally spaced with a distance of 34 mm , double the spacing between the thermocouple measurement positions.

Due to the combustion process the hot gas will be accelerated from injection velocity up to hot gas velocity (320 m/s). Consequently, the static pressure is expected to decrease along the chamber axis. The end of the combustion process will be therefore indicated by the flattening of the pressure gradient. The pressure signals are averaged over the same time interval forehead used for the temperature signals, t_I . Figure 20 and Figure 21 show the static pressure distributions along the chamber axis for different values of chamber pressure and mixture ratios, normalized with the pressure at $x = 272 \text{ mm}$ (PC8), which is the last pressure sensor upstream the throat.

It could be identified a strong pressure gradient of up to the 4% of P_{cc} , for every pressure value P_{cc} and OF . Similar results have been found in previous studies using H_2/LOX propellant combination [15]. As already highlighted from the trend of the temperature signal along the chamber axis, the combustion processes seems to end shortly before the nozzle. An influence of the pressure level and of the mixture ratio on the extension of this area has not been observed during these investigations.

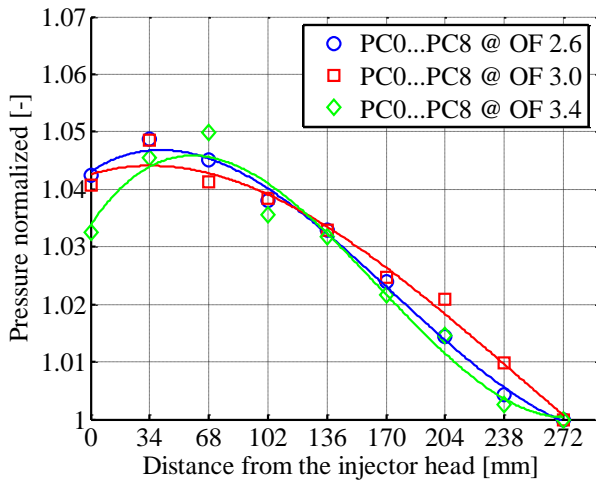


Figure 20: Pressure along the chamber axis for different P_{cc} , $OF = 2.6$

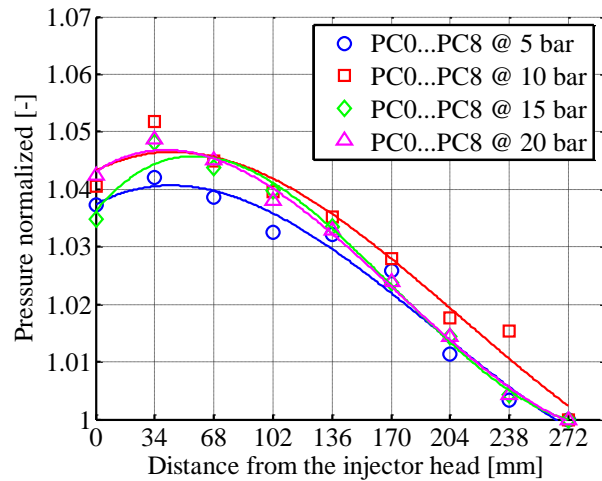


Figure 21: Temperature along the axis for different OF , $P_{cc} = 20 \text{ bar}$

In order to fully characterize the behavior of the shear coaxial injector, C_d values have been calculated over the different load points of the present test campaign, and can be seen in Figure 22. The calculations for the GOX use the inner cross section of the oxygen injection tube as reference area, while the ones for the methane side are based on the effective area of the GCH4 annular gap.

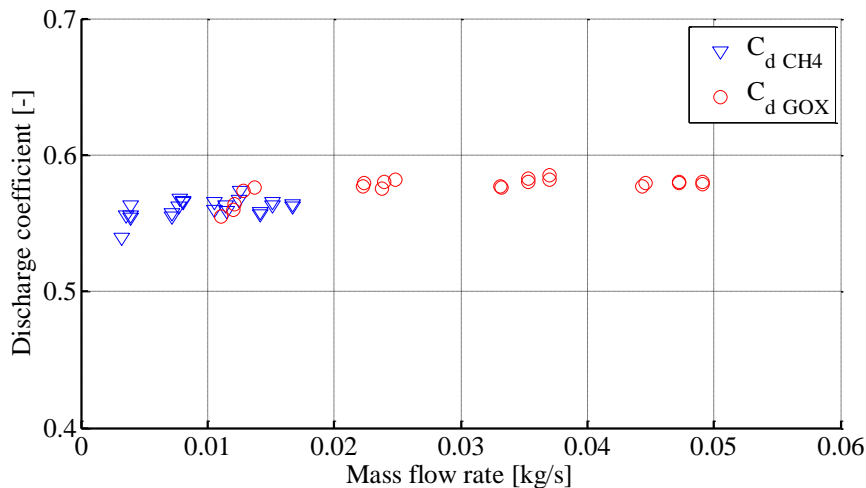


Figure 22: C_d values for different load points

No influence can be seen from changes in combustion chamber pressures or OF . Typical values for the pressure losses at the design point for the oxygen tube are 25% of P_{cc} and of around 22% of P_{cc} for the methane side. The pressure drop is calculated from the manifold pressures upstream the injector element to the combustion chamber pressure closest to the face plate (PC0).

D. Thermtest simulation

The need for a reliable prediction of the thermal behavior of the institute's rocket combustion chambers has led to the development of the engineering tool Thermtest at TUM [12]. Thermtest allows the simulation of steady as well as transient thermal behavior of cooled or uncooled structures over a wide scope of chamber materials and cooling fluids. While the heat conduction inside the chamber material is solved by a 3D finite difference method, the convective heat transfer is implemented by empirical Nusselt correlations. The advantage of this approach is a satisfying accuracy maintaining a reasonably fast simulation of the conjugate heat transfer from the hot gas into the cooling fluid.

Thermtest utilizes 1D hot gas properties acquired from the NASA computer program CEA2 of Sanford Gordon and Bonnie McBride [13]. The temperature of the combustion gases and the ideal characteristic velocity are calculated using the built-in rocket problem. The “injector” level used in this problem case is implied to be right at the injector face plate and “combustion end” at the end of the tubular combustion chamber section. The evolution of temperature caused by reaction kinetics and atomization processes is generally neglected as it is not taken into account in CEA2. The fluid properties needed for heat transfer calculations near the hot chamber wall are calculated assuming an equilibrium composition frozen reactions temperature-pressure-problem. The convective heat transfer from the hot gas to the inner wall, as well as from the wall to the coolant is modeled using different problem specific Nusselt correlations. Thereby, the hot wall heat transfer coefficient is usually calculated from a modified formulation proposed by Sinyarev [16]-[17]. In the past, Thermtest has been validated and adapted for the use of kerosene/oxygen as propellants in small single-element combustion chambers featuring swirl or double swirl coaxial injector elements. Information on Thermtest as well as a comparison with experimental data and calculations from commonly available CFD code has been published [18]-[19].

For the implementation of the propellant combination methane/oxygen, the new injector characteristic and chamber design, efforts have to be done. To account for the multidimensional behavior characterizing the rectangular cross-section of the subscale combustion chamber presented, the code has already been adapted and upgraded, but especially the correct implementation of the heat transfer for the new propellant combination has to be validated. Pressure signals, mass flow rates or OF values, fed directly from the reading of the test data, are the input used for the simulations. Inspired by work of [20], a correction function for the heat load characteristic of generic coaxial injector elements has been applied, in order to take the injector mixing behavior into account. The complete correlation is presented in equation (8). Beside the “fixed” initial heat transfer (“0.2”) and the axial coordinate x , the maximum combustion length l_{max} is the only parameter. The value of l_{max} has been arbitrary chosen equal to combustion length, since the experimental results show that the accomplishment of the combustion process happens on the complete chamber length.

$$\dot{q}_{w,corr} = \dot{q}_w \left(0.2 + 0.8 \tanh \left(\frac{x}{l_{max}} \pi \right) \right) \quad (8)$$

Preliminary simulation results obtained are shown in Figure 23 where it is possible to recognize the characteristic behavior for a heat-sink rocket: the heat flux decreases during the hot run due to the structural temperature increase. Heat flux profile along the chamber axis is plotted in Figure 24. To be noticed the heat flux profile in the nozzle, value that is not possible to reconstruct from experimental data.

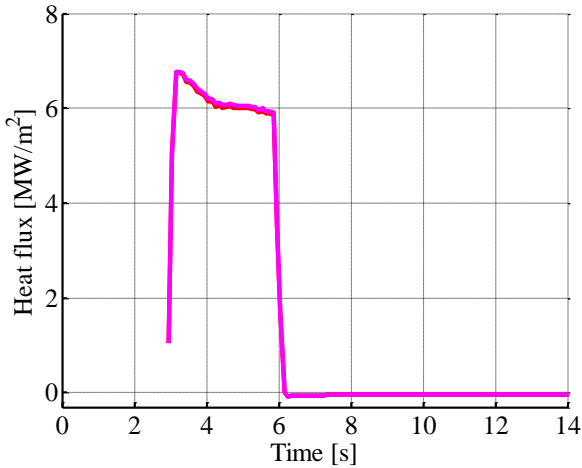


Figure 23: Heat flux vs time in Thermtest

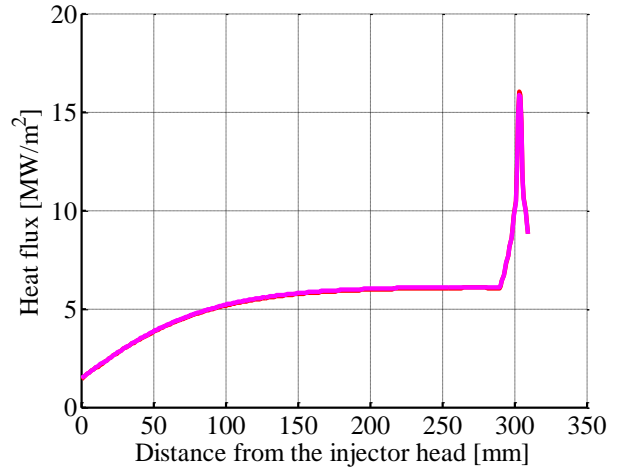


Figure 24: Heat flux profile along chamber axis in Thermtest

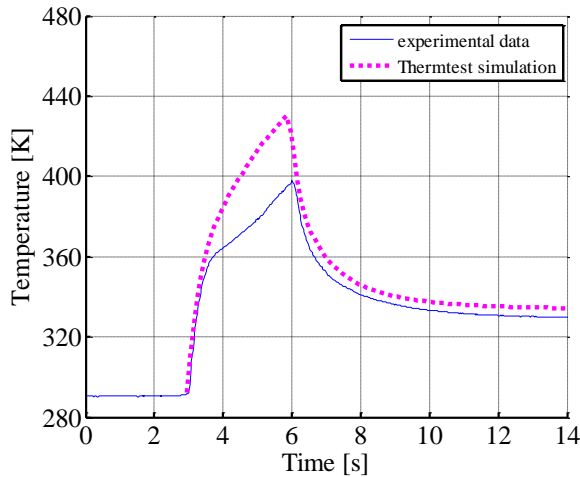


Figure 25: Temperature along the chamber axis in the first segment, tI , Thermtest

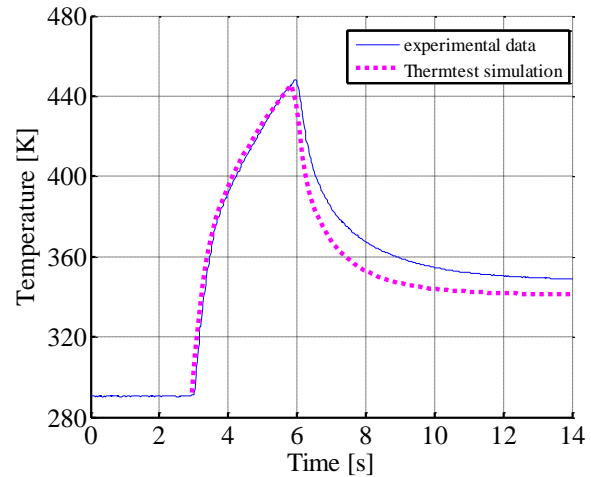


Figure 26: Temperature along the chamber axis in the second segment, tII , Thermtest

Temperature signals, Figure 25 and Figure 26 show an agreement with the experimental data in terms of absolute values and trend especially in the second segment of the combustion chamber. While in the first segment is present a greater disagreement between the simulated data and measured ones.

Conclusion

In the context of the national research program Transregio SFB/TR 40 two multi-injector combustion chambers are designed for GOX and GCH4 propellants research purposes. Before the manufacturing and testing of the aforementioned hardware, a single-element combustion chamber has been designed and tested in order to characterize the injector and to validate the in-house design tool Thermtest.

Detailed wall temperature measurements and derived heat flux data sets have been obtained for GOX/GCH4 single-element shear coaxial injector in a subscale combustion chamber over a range of pressure (5 to 20 bar) and mixture ratio (2.6 to 4.0) conditions. These data sets are valuable for both injector design and code validation. Due to the important multidimensional effects characterizing the geometry of the chamber and the transient nature of the hardware, specific methods for heat flux calculations have been considered. Temperature, heat flux as well as pressure traces show that the combustion process is accomplished towards the end of the chamber. The same trend was observed for all investigated load points. Preliminary simulations, conducted with Thermtest, show good agreement with the experimental results.

An optimization, according to the test data, of the heat transfer model in order to match the injector characteristics is ongoing at TUM. The observed condensation phenomenon will be addressed in more detail in future test campaigns.

Acknowledgment

Part of the present work has been supported by students of the TUM, namely Christian Franzmann and Arne Lampmann. Furthermore, the authors like to thank Christian Bauer for the support provided.

Bibliography

- [1] D.Preclik, G.Hagemann, O.Knab, C.Mäding, D.Haesler, "Lox/Hydrocarbons Preparatory Thrust Chamber Technology Activities in Germany", AIAA-2005-4555, 41st AIAA/ASME/SAE/ASEE Joint Propulsion Conference & Exhibit, July 10th to 13th, 2005, Tucson, Arizona, USA
- [2] J.M.Locke, P.Sibtosh, R.D.Woodward, "Chamber wall heat flux measurements for a LOX/CH4 uni-element rocket", AIAA 2007-5547, 43rd AIAA/ASME/SAE/ASEE Joint Propulsion Conference & Exhibit, July 8th to 11th, 2007, Cincinnati, OH, USA
- [3] A.Kootyev, L.Samoilov, "New engines to power advanced Launch Vehicles", Aerospace Journal, May-June 1998

- [4] G.P.Kalmgkov, S.V.Mosslov “Liquid Rocket Engines working on Oxygen Methane for Space Transportation System of the XXI Century”, IAF-00-5.2.10
- [5] K.Liang, B. Yanf, Z.Zhang, “Investigation of heat transfer and coking characteristics of hydrocarbon fuels”, Journal of Propulsion and Power, Vol. 14, No. 5, September-October 1998
- [6] H.Burkardt, M.Sippel, A.Herbertz, J.Klevanski, “Kerosene vs Methane: A Propellant Tradeoff for reusable liquid booster”, Journal of Spacecraft and Rockets, Vol. 41, No. 5, September-October 2004.
- [7] Götz A., Mäding C., Brummer L., Haeseler D., “Application of Non-Toxic Propellants for Future Advanced Launcher Vehicles”, AIAA 2001-3456, 37th AIAA/ASME/SAE/ASEE Joint Propulsion Conference and Exhibit, Salt LakeCity (Utah), USA
- [8] F.Cuoco, B.Yang, M.Oschwald “experimental investigation of Lox/H₂ and LOX/CH₄ sprays and flames”, 24th International Symposium on Space Technology and Science, Miyzaki, May 2004, ITS 2004-a-04.
- [9] L.Vingert, M.Habiballah, P.Vuillermoz, “Upgrading of the Mascotte cryogenic test bench to the Lox/Methane combustion studies” 4th International Conference on Launcher Technology “Space Launcher Liquid Propulsion”, CNES, Liege, December 2002.
- [10] A.Fröhlich, M.Popp, G.Schmidt, D.Thelmann, “Heat transfer characteristics of H₂/O₂ combustion chambers”, AIAA 93-1826, 29th AIAA/ASME/SAE/ASEE Joint Propulsion Conference, June 28th to 30th, 1993, Monterey, CA, USA
- [11] D.Suslov, A.Woschnak, J.Sender, M.Oschwald, “Test specimen design and measurement technique for investigation of heat transfer processes in cooling channels of rocket engines under real thermal conditions”, AIAA-2003-4613, 39th AIAA/ASME/SAE/ASEE Joint Propulsion Conference & Exhibit, July 20th to 23th, 2003, Huntsville, AL, USA
- [12] Kirchberger, G. Schlieben, O. J. Haidn, “Assessment of Analytical Models for Film Cooling in a Hydrocarbon/ GOX Rocket Combustion Chamber”, AIAA-2012-3909, 48th AIAA/ASME/SAE/ASEE Joint Propulsion Conference and Exhibit, July 29th - August 1st; 2012, Atlanta, GA, USA,
- [13] S.Gordon, B.McBride: “Computer Program for Calculation of Complex Chemical Equilibrium Compositions and Applications”, NASA Reference Publication 1311, 1994.
- [14] L. Hanchoon, K. Moohwan, “The effect of Non-condesable Gas ob Direct Contact Condensation of Steam/Air Mixture”, Journal of the Korean Nuclear Society, Vol. 33, No. 6, pp. 585-595, December, 2001
- [15] D.I.Suslov, R.Arnold, O.J.Haidn „Investigation of Two Dimensional Thermal Loads in the Region Near the Injection Head of a High Pressure Subscale Combustion Chamber, 47th AIAA Aerospace Sciences Meeting Including The New Horions Forum and Aerospace Exposition, January 5-8th 2009, Orlando, Florida
- [16] G.Schmidt: “Technik der Flüssigkeits-Raketentriebwerke“, DaimlerChrysler Aerospace, Munich, 1999.
- [17] Г.Б.Синярев и М.В.Добровольский: “Жидкостные Ракетные Двигатели. Теория и Проектирование.” Москва, 1955
- [18] C.Kirchberger, R.Wagner, H.-P.Kau, S.Soller, P.Martin, M.Bouchez, C.Bonzom, “Prediction and Analysis of Heat Transfer in Small Rocket Chambers.”, AIAA-2008-1260, 46th AIAA Aerospace Sciences Meeting and Exhibit, Reno, NV, USA, January 7th-10th 2008
- [19] M.Bouchez, E.Dufour, F.Cheuret, J.Steelant, P.Grenard, J.Redford, N.Sandham, A.Passaro, D.Baccarella, M.Dalenbring, J. Smith: “Material-Aero-Thermal Interaction Computations in the ATLLAS European Programme”, AIAA-2008-4670, 44th AIAA/ASME/SAE/ASEE Joint Propulsion Conference & Exhibit, , July 21st to 23rd, 2008, Hartford, Connecticut, USA
- [20] A. Ponomarenko, “Thermal Analysis of Thrust Chambers”, 2012